

# Transverse Load Discrimination in Long-Period Fiber Grating via Artificial Neural Network

F. O. Barino<sup>1</sup> , F. S. Delgado<sup>1,2</sup> , A. Bessa dos Santos<sup>1</sup> 

<sup>1</sup> Electrical Engineering Department, UFJF, Juiz de Fora, Brazil

*felipe.barino@engenharia.ufjf.br, alexandre.bessa@engenharia.ufjf.br*

<sup>2</sup> Electrical Department, CEFET-MG, Nepomuceno, Brazil. *felipecdelgado@cefetmg.br*

**Abstract**—We present a general investigation of a Long-Period Grating (LPG) for transverse strain measurement. The transverse strain sensing characteristics, for instance, the load intensity and azimuthal angle, are analyzed with the data set generated by the LPG sensor and probed by artificial neural network (ANN). Furthermore, we evaluate and compare the predictive performance of the interrogation model considering the square correlation coefficient ( $R^2$ ), root mean square error (RMSE) and mean absolute percentage error (MAPE). The results indicate that the ANN model could be successfully employed to estimate the load intensity and azimuthal angle using a single LPG sensor.

**Index Terms**— Artificial neural network, long period grating, optical fiber sensor, transverse load

## I. INTRODUCTION

Long Period Gratings (LPGs) are fiber optic devices, which are extremely important in the field of optical communications [1]-[3] and instrumentation [4]-[7]. Concerning sensing applications, the transverse load characteristic is an extremely important mechanical feature of LPGs. Some previous research focused on the investigation of their behavior under transverse load effect. In this context, [8], [9] conducted experiments using LPGs inscribed by UV laser and reported that the attenuation band of the grating was split into two sub dips with the increased transverse load. Use of CO<sub>2</sub> laser induced LPGs are also reported for transverse load [10]. Whereas in [11], the authors showed that the sensitivity of the LPGs produced by the CO<sub>2</sub> laser technique strongly depends upon load orientation. Thus, the intrinsic response of LPGs to transverse load imposes serious implications for the discrimination of transverse load and it is important to remark that it is a nonlinear problem, since the load orientation affects LPG's sensitivity to the load itself.

In order to ensure an appropriate monitoring load and angle, more than just a LPG sensor could be required, since this scenario can be interpreted as two-dimensional load sensing. But taking advantage

of dip splitting and orientation dependence on LPG's sensitivity to load, one can build a single LPG sensor for two dimensional load field. Therefore, it is extremely important to couple the LPG sensing capabilities with reliable regression methods, in order to determine both the load and its angle of incidence.

In this work, resonant wavelength shifts of an electric arc-induced LPG sensor due to transverse load are investigated. We introduce artificial neural network (ANN) to process the LPG spectrum and estimate the intensity and angle of an applied force. Therefore, the ANN method establishes a relationship between the LPG spectral data and different transverse load conditions. Then, we analyzed the results of the developed artificial neural network based on square correlation coefficient ( $R^2$ ), root mean square error (RMSE) and mean absolute percentage error (MAPE) and, finally, the results indicated that the ANN could be successfully used for estimating load intensity and its angle of incidence.

## II. METHODS

Long Period Gratings are optical devices that promote energy coupling between the fundamental core mode and co-propagating cladding modes. The transmission spectrum of those devices contains a series of attenuation bands located at different resonant wavelengths  $\lambda^i$ , which correspond to energy coupling to various cladding modes. The phase-matching condition for this energy coupling can be expressed as, [12]:

$$\lambda_i = (n_{eff,co} - n_{eff,cl}^i)\Lambda \quad (1)$$

where  $n_{eff,co}$  and  $n_{eff,cl}^i$  are the effective refractive indices of the core and cladding modes, respectively, and  $\Lambda$  represents the period of the grating. Generally, arc-induced LPGs has an inhomogeneous refractive index profile within the fiber cross-section, due to grating fabrication process [13]-[15], which induces birefringence in the grating structure. Thus, grating properties such as resonant wavelength and amplitude peak, for example, depends upon the state of polarization (SOP) of light incident on the fiber grating. For a birefringent LPG, we may assume the refractive index of birefringence of the optical axes  $f$  and  $s$  to be  $n_f$  and  $n_s$ , respectively, with  $n_f < n_s$ . Then, the corresponding orthogonal polarization propagation constants are given by [16]:

$$\beta_f = \frac{2\pi n_f}{\lambda} \quad (2)$$

$$\beta_s = \frac{2\pi n_s}{\lambda} \quad (3)$$

the combination of the propagation constants of these two polarization axes,  $\beta_f$  and  $\beta_s$ , determines the propagation constant of the propagating mode. Thus, it is worth noting that both  $\beta_f$  and  $\beta_s$  exerts strong influence on mode coupling, which modifies the amplitude and wavelength of resonant dip.

Furthermore, the effect of transverse load in LPGs produces a new linear birefringence in the optical fiber, due to photoelastic effect [16], which modifies the original fast and slow axes propagation constant. Therefore, changes in the phase difference in Eq. (1) and in the coupling between waveguide's core and cladding modes are consequences of the applied transverse load. Finally, each resonant peak in transmission spectra are split into two sub peaks, corresponding to two principal states of polarization [9].

Thus, spectral characteristics of those two principal states of polarization can be used in transverse load sensing. In order to resolve the nonlinearities of transverse load and correlate it to the load intensity and angle we propose the use of ANN. Although the response of LPGs to transverse load at different incidence angles is reported in literature [10], [11], practical means of correlating spectrum with the load itself are not addressed in those works.

The use of ANN in LPG multiple parameter sensing is well described in [17], where the authors presents the use of an ANN to probe both curvature and its orientation on a bending sensor, using LPG's spectral data as input of the system. ANNs are suitable for this task due to its ability to map input/output from measured data using knowledge acquired in a learning phase [18], [19].

There are several types of ANN algorithms, and the back-propagation (BP) multilayer perceptron (MLP) is an important type of neural network, capable of performing input/output mapping to achieve function regression using a single hidden layer, according to the universal approximation theorem [20]. Therefore, two MLPs were developed in this work, one for load intensity estimation ( $L$ ) and another for its incidence angle ( $\theta$ ), separately.

The structure of those ANNs can be seen on Fig. 1 and they were implemented in python with aid of scikit-learn library [21]. Both models are three layers perceptron, those layers are: input layer, hidden layer and output layer. The input layer has two neurons, for the resonant wavelength of the two principal states of polarization,  $\lambda_{p1}$  and  $\lambda_{p2}$ , and the output layer has a single neuron. Furthermore, the number of neurons in the hidden layer was investigated, varying its size from 10 to 200 neurons. We performed the model selection by trial and error for 20 different hidden layer sizes, training each configuration ten times. Mean error for each one of these configurations was taken into account, to reduce initial weights impact on the final result, when choosing the proper hidden layer size. Finally, we choose the configuration that presented best generalization, as discussed on section IV.

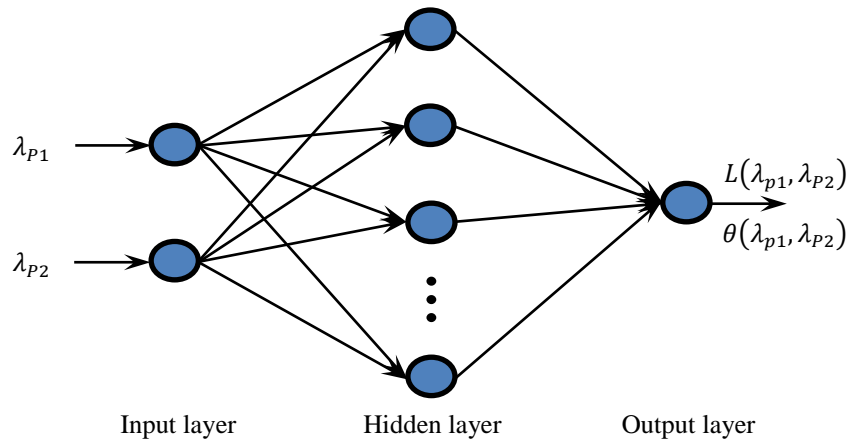


Fig. 1. Structure of a three layer BP neural network.

The output of the  $i^{th}$  neuron in the hidden layer ( $H_i$ ) is given by:

$$H_i = f(\lambda_{p1}w_{i,1} + \lambda_{p2}w_{i,2}) \quad (4)$$

where  $w_{i,1}$  and  $w_{i,2}$  are the weight values on the connection between the inputs  $\lambda_{p1}$  and  $\lambda_{p2}$ , respectively, and the  $i^{th}$  neuron from the hidden layer, and  $f(\cdot)$  is the neuron's activation function, Rectified Linear Unit (ReLU) in the case of this work.

For a regression problem the output values are real valued numbers. Thus, we adopt no activation function in the output layer, in order to approximate any possible real value. The values of load intensity and angle of incidence in the output layer are related to the  $i^{th}$  neuron in the hidden layer by:

$$L = \sum w_{1,i} H_i \quad (5)$$

$$\theta = \sum w_{1,i} H_i \quad (6)$$

where  $w_{1,i}$  are the weight data between  $H_i$  in the hidden layer and the output from the output layer of the ANN.

In what concerns the training process, two different datasets were used to train the ANNs, with input-output pairs  $\{(\lambda_{p1}, \lambda_{p2}), (L)\}$  and  $\{(\lambda_{p1}, \lambda_{p2}), (\theta)\}$ . The former is used to train a network for load intensity estimation and the latter to train a model for estimating its incidence angle. Furthermore, we split both datasets into two subsets: train and test, for training and evaluating the models, respectively. In order to perform the weights optimization, aiming to reduce estimation error, we use ADAM optimizer, since it's reported to have a great performance and fast convergence in MLP training [22]. Finally, the nonlinear function can be approximated and, therefore, allowing us to recover the intensity and angle of incidence of the LPG sensor applied load.

### III. EXPERIMENTAL SETUP

Fig. 2 shows the schematic representation of the experimental setup for testing LPG under different

transverse load scenarios. Broadband light source (BBS), with central wavelength near 1550 nm, is used alongside with an optical spectrum analyzer (OSA), to acquire the spectrum during the transverse load tests. In this experimental configuration, light from the broadband source is polarized using a fiber polarizer and the state of polarization (SOP) can be adjusted by the polarization controller (PC). Furthermore, a LPG sensor with grating period of  $\Lambda = 500 \mu\text{m}$ , fabricated using the electric arc technique [23], is placed with both ends fixed in two fiber rotators between the PC and the OSA.

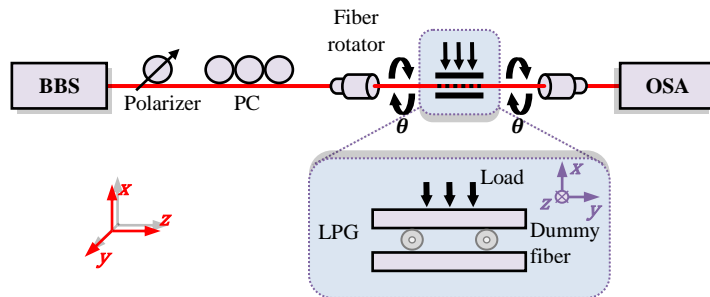


Fig. 2. Experimental configuration of the transverse load sensor.

To characterize LPG's response to different transverse load directions, the device was synchronously rotated around fiber axis, using the fiber rotators. The LPG was laid between two flat surface plates with an auxiliary dummy fiber for balance, which is represented in Fig. 2 inset. It is worth noting that the dummy fiber ensures that a constant even load is applied to the fiber during the experiment, which was performed with constant temperature at 25 °C.

The experiment consists in the application of five different loads for 12 different incidence angles. We increase the load intensity from 0 kg (free load) to 5 kg in equally spaced steps, whereas its angle varied by  $\theta = 30^\circ$  until a full turn. Under all circumstances LPG is probed with polarized lights, defined as Polarization 1 (P1) and Polarization 2 (P2), and with random polarized light, for the sake of comparison. Resonant wavelength at both states of polarization (P1 and P2) was recorded to build the dataset used in ANN development.

#### IV. RESULTS AND DISCUSSION

During the experimental tests, birefringence in the grating structure induced by the transverse loading was immediately observed in the spectrum. Thus, the grating exhibited a pronounced resonant band split effect, which resulted in two sub peaks corresponding to the two orthogonal polarization states.

Fig. 3(a) shows the grating response under free load and

Fig. 3(b) the relationship between load (intensity and angle) and resonant wavelength, for

Polarization 1 and Polarization 2, also named  $\lambda_{P1}$  and  $\lambda_{P2}$ , respectively.

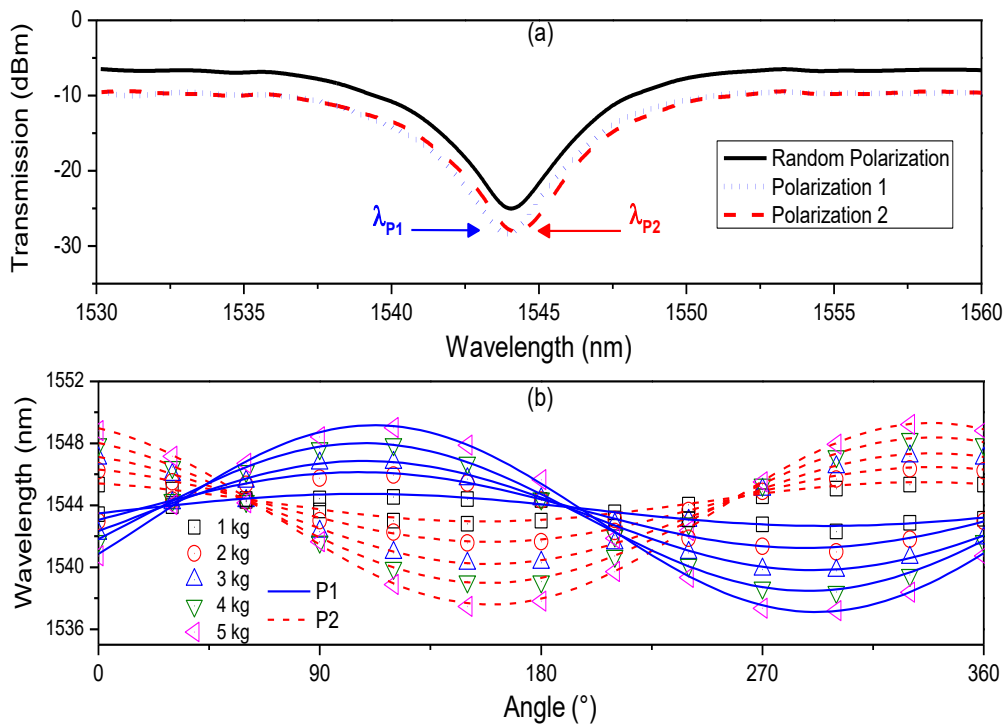


Fig. 3. a) LPG's transmission spectra under free load, b) Resonant wavelength for different load-angle combinations.

Fitting the experimental data as a function of the incidence angle we obtain the blue (dashed) and red (dotted) lines in

Fig. 3(b), which represents  $\lambda_{P1}$  and  $\lambda_{P2}$ , respectively. The periodic dependence of dips' position on load direction can be easily seen. Note that amplitude grows with load intensity, leading to observed sub peaks in spectrum, and that sensitivity is highly influenced by application angle, as shown in Fig. 4, confirming the system's nonlinear behavior.

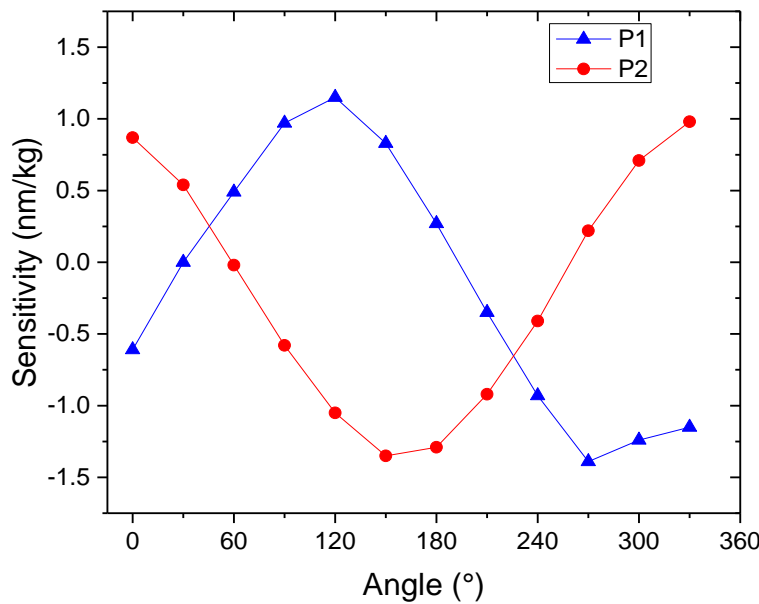


Fig. 4. Load sensitivity as function of the incidence angle.

As discussed in section II, 20 models with different hidden layer sizes we tested to determine the best ANN configuration. The result is shown in Fig. 5, where RMSE for train and test sets are displayed for both models. In Fig. 5(a) load intensity estimation RMSE for different number of neurons is plotted and the selected size highlighted, the same graph is shown in Fig. 5(b), but for angle of incidence estimation.

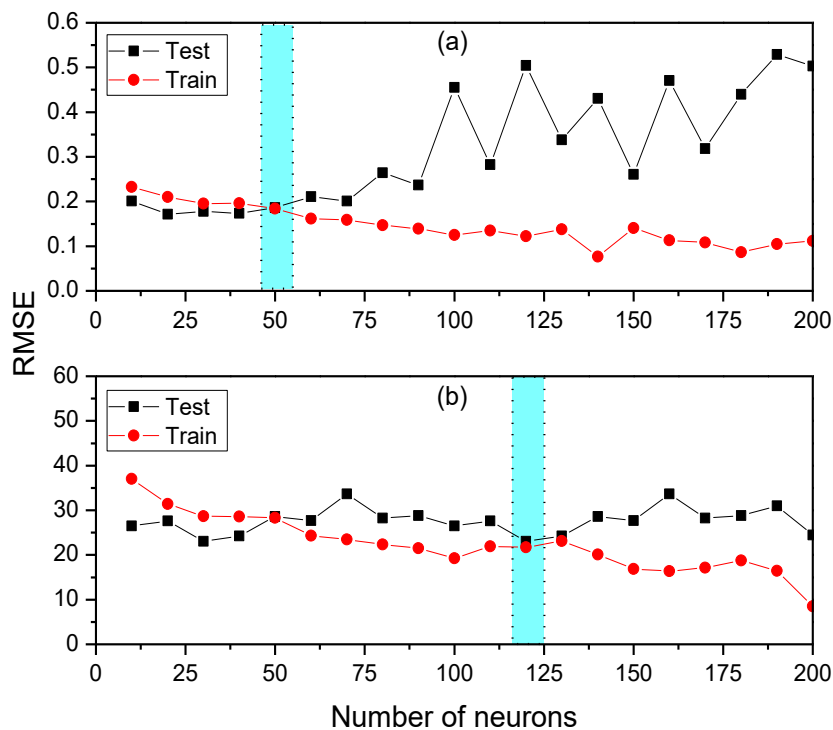


Fig. 5. Number of neurons in the hidden layer: a) Load intensity ANN and b) Angle of incidence ANN.

Note that the choice of hidden layer size is a tradeoff between train and test performance, in order

to avoid overfitting. Therefore, we chose 50 neurons for the load estimation model and 120 neurons for the angle of incidence ANN, since for those values minimum train RMSE is achieved without a trend growth in test RMSE.

Performance of the final models can be seen in Fig. 6, which ANNs' response for train and test data is presented. The  $x$ -axis shows the target value, while the  $y$ -axis represents the model output. Therefore, it is possible to observe the relationship between ANNs output and experimental measurements.

In order to analyze the performance of the proposed models, we consider the RMSE, MAPE and the coefficient of determination ( $R^2$ ), for training and test datasets. One can observe that values of  $R^2$  greater than 90% were achieved for both ANN models developed, as shown in Table I. Therefore, indicating a good agreement between the estimated and experimental results. We can further observe that RMSE for the developed models were found to be low in both models, as well as the MAPE (normalized by the maximum value). Thus, confirming that the ANNs could be successfully used to discriminate the transverse load applied to the optical fiber sensor. Moreover, the proposed method can be used in single LPG bidimensional force sensing, since it can estimate load intensity/direction, therefore representing a 2D force field in polar coordinates.

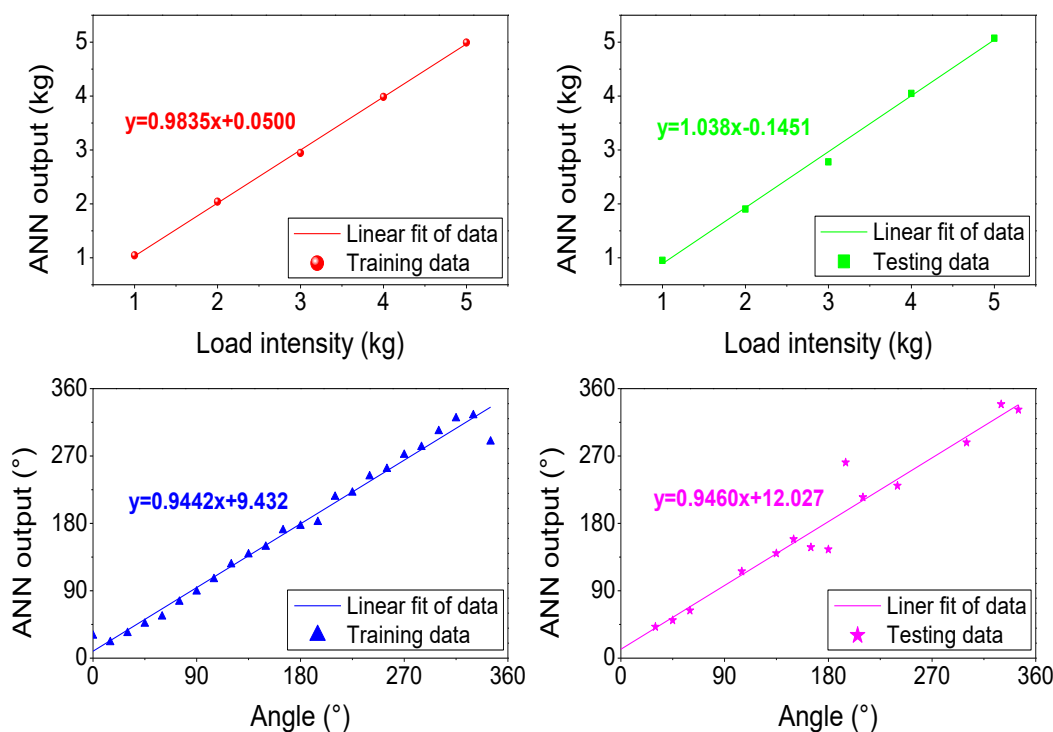


Fig. 6. Experimental values against ANN prediction for load intensity and angle of incidence.

TABLE I. ANN MODELS PERFORMANCE EVALUATION.

	Load Intensity		Angle of Incidence	
	Training	Testing	Training	Testing
RMSE	0.031	0.047	550.5	586.7
MAPE	1.724%	3.495%	2.474%	5.055%
R <sup>2</sup>	0.984	0.923	0.950	0.935

## V. CONCLUSION

Two different ANNs were developed to discriminate the complex and nonlinear behavior of the transverse load applied to the LPG sensing system. The method is based upon the measurement of the resonant wavelength responses of the two principal states of polarization,  $\lambda_{p1}$  and  $\lambda_{p2}$ , which presents different responses to the applied transverse load. Then, we used BP neural networks to realize the regression and achieve the prediction of load and intensity and angle of incidence. Finally, results showed that using the proposed models coupled to LPG sensor, it is possible to calibrate and monitor simultaneously the intensity and angle of incidence of an applied load. Therefore, improving data analysis and promoting the development of practical interrogation equipment of optical load sensors.

## ACKNOWLEDGMENTS

The authors acknowledge the financial support in part of CAPES - Coordenação de Aperfeiçoamento de Pessoal de Nível Superior, CNPq - Conselho Nacional de Desenvolvimento Científico e Tecnológico, INERGE - Instituto Nacional de Energia Elétrica, FAPEMIG - Fundação de Amparo à Pesquisa no Estado de Minas Gerais and Santo Antônio Energia.

## REFERENCES

- [1] A. Hasegawa-Urushibara, T. Mori, T. Sakamoto and M. Wada, "Experimental verification of mode-dependent loss reduction by mode coupling using long-period grating," in *2017 Optical Fiber Communications Conference and Exhibition (OFC)*, Los Angeles, CA, 2017, pp. 1-3.
- [2] Y. Guo, Y. Liu, Z. Wang, Z. Wang and H. Zhang, "All-fiber mode-locked cylindrical vector beam laser using broadband long period grating," *Laser Physics Letters*, vol. 15, no. 8, pp. 085108, 2018.
- [3] F. Delgado and A. dos Santos, "Reduction of intrinsic polarization dependence in arc-induced long-period fiber gratings," *Optical Engineering*, vol. 57, no. 06, p. 1, 2018.
- [4] J. Zhang, Y. Zhang, L. Zhang, W. Zhang, L. Wang and T. Yan, "Two-axis bending vector sensor based on a long-period fiber grating cascading with a hump-shaped taper," *Measurement Science and Technology*, vol. 29, no. 9, pp. 095107, 2018.
- [5] F. Delgado and A. Bessa, "Torsion-dependent spectral response of long-period fiber grating based on electric arc technique with axial rotation of the fiber," *Microwave and Optical Technology Letters*, vol. 61, no. 1, pp. 178-181, 2018.
- [6] W. Zhang, J. Hao, X. Lou, M. Dong and L. Zhu, "All-Fiber Dual-Parameter Sensor Based on Cascaded Long Period Fiber Grating Pair Fabricated by Femtosecond Laser and CO<sub>2</sub> Laser," *Fiber and Integrated Optics*, vol. 37, no. 2, pp. 66-78, 2018.

- [7] D. Hou et al., "Fiber sphere-embedded long-period fiber grating for curvature measurement with high sensitivity," *Optical Engineering*, vol. 57, no. 04, pp. 1, 2018.
- [8] Y. Liu, L. Zhang and I. Bennion, "Fibre optic load sensors with high transverse strain sensitivity based on long-period gratings in B/Ge co-doped fibre," *Electronics Letters*, vol. 35, no. 8, pp. 661, 1999.
- [9] L. Zhang, Y. Liu, L. Everall, J. Williams and I. Bennion, "Design and realization of long-period grating devices in conventional and high birefringence fibers and their novel applications as fiber-optic load sensors," *IEEE Journal of Selected Topics in Quantum Electronics*, vol. 5, no. 5, pp. 1373-1378, 1999.
- [10] Y. Rao, Y. Wang, Z. Ran and T. Zhu, "Novel fiber-optic sensors based on long-period fiber gratings written by high-frequency CO<sub>2</sub> laser pulses," *Journal of Lightwave Technology*, vol. 21, no. 5, pp. 1320-1327, 2003.
- [11] Y. Wang, D. Wang, W. Jin and Y. Rao, "Asymmetric transverse-load characteristics and polarization dependence of long-period fiber gratings written by a focused CO<sub>2</sub> laser," *Applied Optics*, vol. 46, no. 16, pp. 3079, 2007.
- [12] S. James and R. Tatam, "Optical fibre long-period grating sensors: characteristics and application," *Measurement Science and Technology*, vol. 14, no. 5, pp. R49-R61, 2003.
- [13] Y. Wang, D. Wang, W. Jin and Y. Rao, "Asymmetric transverse-load characteristics and polarization dependence of long-period fiber gratings written by a focused CO<sub>2</sub> laser," *Applied Optics*, vol. 46, no. 16, pp. 3079, 2007.
- [14] B. Bachim and T. Gaylord, "Polarization-dependent loss and birefringence in long-period fiber gratings," *Applied Optics*, vol. 42, no. 34, pp. 6816, 2003.
- [15] G. Rego, J. Santos and H. Salgado, "Polarization dependent loss of arc-induced long-period fibre gratings," *Optics Communications*, vol. 262, no. 2, pp. 152-156, 2006.
- [16] H. Liu, D. Liang, X. Han and J. Zeng, "Long period fiber grating transverse load effect-based sensor for the omnidirectional monitoring of rebar corrosion in concrete," *Applied Optics*, vol. 52, no. 14, pp. 3246, 2013.
- [17] R. Costa, G. Possetti, L. de Arruda, M. Muller and J. Fabris, "Curvature vector smart sensing with a long-period fibre grating probed by artificial intelligence," *Measurement Science and Technology*, vol. 21, no. 9, pp. 094027, 2010.
- [18] P. Simpson, *Artificial neural systems*, 1st ed. New York: MacGraw-Hill, 1991.
- [19] D. Patterson, *Artificial neural networks : theory and applications*. Singapore: Prentice Hall, 1996.
- [20] K. Hornik, M. Stinchcombe and H. White, "Multilayer feedforward networks are universal approximators," *Neural Networks*, vol. 2, no. 5, pp. 359-366, 1989.
- [21] F. Pedregosa et al., "Scikit-learn: Machine Learning in Python," *Journal of Machine Learning Research*, 2825-2830, 2011.
- [22] D. Kingma and J. Ba, "Adam: A Method for Stochastic Optimization," in *3rd International Conference for Learning Representations*, 2014.
- [23] G. Rego, P. Marques, J. Snatos and H. Salgado, "Arc-Induced Long-Period Gratings," *Fiber and Integrated Optics*, vol. 24, no. 3-4, pp. 245-259, 2005.